Critical exponents of the classical three-dimensional Heisenberg model: A single-cluster Monte Carlo study

Christian Holm
Institut für Theoretische Physik, Freie Universität Berlin, Arnimallee 14, D-1000 Berlin 33, Germany

Wolfhard Janke
Höchstleistungsrechenzentrum, Forschungszentrum Jülich, Postfach 1913, D-5170 Jülich, Germany
(Received 4 January 1993)

We have simulated the three-dimensional Heisenberg model on simple cubic lattices, using the single-cluster Monte Carlo update algorithm. The expected pronounced reduction of critical slowing down at the phase transition is verified. This allows simulations on significantly larger lattices than in previous studies and consequently a better control over systematic errors. In one set of simulations we employ the usual finite-size scaling methods to compute the critical exponents $\nu,\alpha,\beta,\gamma,\eta$ from a few measurements in the vicinity of the critical point, making extensive use of histogram reweighting and optimization techniques. In another set of simulations we report measurements of improved estimators for the spatial correlation length and the susceptibility in the high-temperature phase, obtained on lattices with up to 100^3 spins. This enables us to compute independent estimates of ν and γ from power-law fits of their critical divergencies.

I. INTRODUCTION

Critical exponents are the distinguishing parameters characterizing continuous phase transitions. Most theoretical estimates of their values have been calculated along three different routes: first, with the assumption of universality, from (resummed) perturbation expansions of generic field-theoretical models; second, from high-temperature series expansions of lattice models; and third, from Monte Carlo (MC) simulations of the associated Boltzmann distributions. All these approaches are based on resummation or extrapolation techniques whose systematic errors are difficult to control. To gain confidence in the numerical values of the exponents, it is therefore quite important to have several independent approaches for the cross-checks available.

Until a few years ago, the precision of Monte Carlo estimates was comparatively poor, since this approach was plagued not only by systematic but also by statistical errors. The problem is that MC algorithms based on *local* update procedures are severely hampered near criticality by extremely long autocorrelation times (so-called critical slowing down), which reduce the effective statistics and thus increase the statistical errors considerably.[1] The recent development[2] of *nonlocal* update algorithms that overcome the problem of critical slowing down is a major step forward. It is this algorithmic improvement combined with the higher speed of modern computers that makes systematic tests of finite-size scaling (FSS) predictions[3] and a reliable computation of critical exponents much more feasible than a few years ago.

For spin systems, cluster algorithms[4,5] turned out to be particularly successful. Recent applications of the multiple[4] and single[5] cluster variants to two-dimensional (2D) Ising,[6–8] XY,[9–12] Heisenberg,[13,14] and other $O(n)$ models[15] have demonstrated that both variants are equally good tools to simulate these 2D systems. In three dimensions (3D), however, extensive tests for the Ising[6,7,16] and XY (Refs. 17 and 18) models clearly showed that the single-cluster variant is the superior algorithm. In our study of the 3D Heisenberg model, we have therefore chosen the single-cluster update algorithm.[19] The setup of our simulations is described in some detail in Sec. II.

There are of course many sources for a comparison with simulations based on the standard local heat-bath[20] or Metropolis[21,22] algorithm. In a recent series of papers, Peczak, Ferrenberg, and Landau[23,24] used the latter algorithm combined with histogram reweighting techniques[25–28] to estimate the critical coupling and the critical exponents of the 3D Heisenberg model from a FSS analysis of simulations on simple cubic lattices[23] and investigated also its (exponential) autocorrelation time τ_0.[24] Their result, $\tau_0 \propto L^z$, with dynamical critical exponent $z=1.94(6)$, shows that τ_0 is rapidly increasing with the linear lattice size L and explains why they could not go to systems larger than 24^3. Since, as expected, the autocorrelation time for the single-cluster algorithm turns out to be almost independent of L, we could study much larger lattices of size up to 48^3 in reasonable computer time. Our results described in Sec. III provide evidence that the asymptotic FSS region is indeed reached quite early or, in other words, that the amplitudes of correction terms are very small. The present study thus significantly reduces the danger of systematic errors in the MC estimates of critical exponents from FSS analyses.

In Sec. IV we report another set of high-precision simulations, done this time in the high-temperature phase. There we use variance reduced "cluster estimators"[14] for the spatial correlation length ξ and the susceptibility χ. By going to very large systems with up to 100^3

spins, we have made sure that these data have only negligible finite-size corrections well below the statistical errors of about 0.2%. Least-squares fits of the critical divergencies of ξ and χ to the well-known power laws yield independent estimates for the critical coupling and the critical exponents ν and γ. Obviously, this is another useful check on residual systematic errors. Finally, in Sec. V, we briefly discuss and summarize our main results.

II. MODEL AND SIMULATION TECHNIQUES

Let us start with a brief description of the model and some remarks on the simulation techniques we have used. The partition function of the Heisenberg model is given by

$$Z=\prod_{\mathbf{x}}\left[\int\frac{d\phi(\mathbf{x})d\cos\theta(\mathbf{x})}{4\pi}\right]e^{-\beta E}, \tag{1}$$

where $\beta\equiv J/k_BT$ is the (reduced) inverse temperature and the energy is

$$E=\sum_{\mathbf{x},i}[1-\vec{s}(\mathbf{x})\vec{s}(\mathbf{x}+\mathbf{i})]. \tag{2}$$

Here $\vec{s}=(\sin\theta\cos\phi,\ \sin\theta\sin\phi,\ \cos\theta)$ are three-dimensional unit spins at the sites $\mathbf{x}$ of a simple cubic lattice of size $V\equiv L^3$ and $\mathbf{i}$ are unit steps in the three coordinate directions. We always employ periodic boundary conditions.

A. Algorithm

For the closely related 3D Ising and XY models it has been shown[6,16–18] that the single-cluster update is the fastest MC algorithm available. We have therefore chosen this variant for our study of the 3D Heisenberg model. One update in the single-cluster variant consists of choosing a random mirror plane and a random site, which is the starting point for growing a cluster of reflected spins. The size and shape of the cluster are controlled by a Metropolis-like accept-reject criterion satisfying detailed balance.[5,9] Compared with the multiple-cluster algorithm, this variant is technically somewhat simpler to implement and, more importantly, in three dimensions numerically more efficient. The reason is that, on the average, larger clusters are moved.

To test the performance of the algorithm, we have recorded autocorrelation functions $A(k)=\rho(k)/\rho(0)$, with

$$\rho(k)=\langle O_iO_{i+k}\rangle-\langle O_i\rangle^2, \tag{3}$$

and O_i denoting the ith measurement of an observable. We have focused on the integrated autocorrelation time $\tau\equiv\frac{1}{2}+\sum_{k=1}^{\infty}A(k)$, which describes the enhancement of the statistical error $\varepsilon=\sqrt{\sigma^2/N}\sqrt{2\tau}$ for the mean value over a sample of N correlated measurements of variance σ^2. The infinite sum was always self-consistently cut off at $k_{\max}\approx 6\tau$.[29–31]

Recall that for the single-cluster update some care is necessary in defining the unit of time, since in each update step only a relatively small fraction of the spins is moved, depending on temperature and lattice size. More precisely, our results show that near β_c and for all lattice sizes the average cluster size $\langle|C|\rangle$ is proportional to the susceptibility,

$$\langle|C|\rangle\approx 0.75\bar{\chi} \tag{4}$$

(with roughly the same constant as in two dimensions[14]), where $\bar{\chi}=\chi/\beta=V\langle\mathbf{m}^2\rangle$, $\mathbf{m}=(1/V)\sum_{\mathbf{x}}\vec{s}(\mathbf{x})$. At β_c, the susceptibility behaves like $\chi\propto L^{\gamma/\nu}=L^{2-\eta}$ (with very small $\eta\approx 0.04$), so that with increasing lattice size the fraction of moved spins in each update step decreases like $\langle|C|\rangle/V\propto L^{-(1+\eta)}$, i.e., roughly $\propto 1/L$. Since the CPU time needed for a single-cluster update is approximately proportional to the number of moved spins, it is convenient to use $N_0\equiv V/\langle|C|\rangle\propto L^{1+\eta}$ single update steps as unit of time. This is then directly comparable with other schemes that attempt moves for all spins in one update step. All our autocorrelation times refer to this unit of time (Metropolis-equivalent unit), which can always be achieved by a rescaling of the time variable.

For the susceptibility we typically find $\tau\approx 1.5$–2.0. The values of τ for each simulation are given in Table I. Already our rough estimate of τ shows that for large system sizes the single-cluster update clearly outperforms the Metropolis algorithm, for which the exponential autocorrelation time τ_0 has recently been determined[24] to be $\tau_0=aL^z$, with amplitude[32] $a\approx 3.76$ and dynamical critical exponent $z=1.94(6)$. For our largest lattice size $L=48$, this implies a reduction of the autocorrelation

TABLE I. Measurement statistics: N is the number of measurements, taken after $f\times L^3$ spins are flipped (on the average), $\langle|C|\rangle$ is the average cluster size that is measured after each update step, and τ is a rough estimate of the autocorrelation time in Metropolis-equivalent units.

L	β	N	f	$\langle\|C\|\rangle$	τ
12	0.6783	1430249	0.045	79	0.8
12	0.6929	5222274	0.071	122	1.2
12	0.7009	931277	0.086	149	1.4
16	0.6872	242804	0.122	167	1.4
16	0.6929	217393	0.157	213	1.8
16	0.6953	206676	0.174	241	1.9
20	0.6862	270067	0.110	220	1.1
20	0.6929	332725	0.208	332	1.8
20	0.6947	284544	0.184	369	1.8
24	0.6872	709711	0.130	300	1.0
24	0.6929	472831	0.207	476	1.6
24	0.6953	350379	0.244	563	1.7
24	0.6972	355572	0.274	631	1.7
32	0.6881	356881	0.126	460	1.1
32	0.6929	351394	0.206	842	1.8
32	0.6965	360726	0.215	1174	1.9
40	0.6904	255563	0.106	851	1.1
40	0.6929	216251	0.163	1304	1.5
40	0.6953	232234	0.194	1774	1.8
48	0.6914	131620	0.145	1339	1.2
48	0.6929	138729	0.200	1840	1.6
48	0.6941	126643	0.165	2287	1.6
48	0.6968	174441	0.178	3287	1.7

time by about three orders of magnitude. A more detailed study of the autocorrelations is in preparation.

To extract the critical exponents, we have performed two sets of simulations: one in the critical region where the correlation length of the infinite system is much larger than the linear system size, $\xi_\infty \gg L$, and the other in the high-temperature phase, making sure that $\xi_\infty \ll L$ to reduce finite-size corrections as much as possible. The quantities we have measured are the internal energy, specific heat, correlation length, average cluster size, susceptibility, and higher-order moments. In the critical region this can be done most efficiently by combining the single-cluster update with multihistogram sampling techniques and in the high-temperature phase by using improved estimators for measurements.

B. Improved estimators

An improved "cluster estimator" for the spin-spin correlation function in the high-temperature phase, $G(\mathbf{x}-\mathbf{x}') \equiv \langle \vec{s}(\mathbf{x})\cdot\vec{s}(\mathbf{x}')\rangle$, is given by[14]

$$\tilde{G}(\mathbf{x}-\mathbf{x}') = 3\frac{V}{|C|}\vec{r}\cdot\vec{s}(\mathbf{x})\vec{r}\cdot\vec{s}(\mathbf{x}')\Theta_C(\mathbf{x})\Theta_C(\mathbf{x}') , \tag{5}$$

where $\vec{r}$ is the normal of the mirror plane used in the construction of the cluster of size $|C|$ and $\Theta_C(\mathbf{x})$ is its characteristic function ($=1$ if $\mathbf{x}\in C$ and 0 otherwise). For the Fourier transform $\hat{G}(\mathbf{k}) = \sum_{\mathbf{x}} G(\mathbf{x})\exp(-i\mathbf{k}\cdot\mathbf{x})$, this implies the improved estimator

$$\tilde{\hat{G}}(\mathbf{k}) = \frac{3}{|C|}\left[\left[\sum_{\mathbf{x}\in C}\vec{r}\cdot\vec{s}(\mathbf{x})\cos\mathbf{k}\cdot\mathbf{x}\right]^2 + \left[\sum_{\mathbf{x}\in C}\vec{r}\cdot\vec{s}(\mathbf{x})\sin\mathbf{k}\cdot\mathbf{x}\right]^2\right] , \tag{6}$$

which, for $\mathbf{k}=\mathbf{0}$, reduces to an improved estimator for the susceptibility $\bar{\chi}$ in the high-temperature phase,

$$\tilde{\hat{G}}(\mathbf{0}) = \tilde{\bar{\chi}} = \frac{3}{|C|}\left[\sum_{\mathbf{x}\in C}\vec{r}\cdot\vec{s}(\mathbf{x})\right]^2 . \tag{7}$$

Note that we follow in the definition of the susceptibility $\bar{\chi}$ in the high-temperature section the standard convention of omitting the β factor. From the theoretically expected small-k behavior of the inverse Fourier transform

$$\hat{G}(\mathbf{k})^{-1} = c\left[\sum_{i=1}^{3} 2(1-\cos k_i) + (1/\xi)^2\right] \approx c[\mathbf{k}^2 + (1/\xi)^2] , \tag{8}$$

where c is a constant and $k_i = (2\pi/L)n_i$, $n_i = 1,\ldots,L$, one may extract the correlation length ξ by measuring $\hat{G}$ for a few long-wavelength modes and performing least-squares fits to (8). In our simulations we have measured $\hat{G}(\mathbf{k})$ for $\mathbf{n}=(0,0,0)$, (1,0,0), (1,1,0), (1,1,1), (2,0,0), and (2,1,0) (see Sec. IV). It is well known that by means of the estimators (5)–(7) a significant reduction of variance can *only* be expected outside the FSS region where the average cluster size is small compared with the volume of the system.

C. Histogram techniques

Even though histogram reweighting techniques have been known for a long time,[25] they have gained increasing popularity as a practical tool only quite recently.[26] The best performance is achieved *near* criticality, and in this sense the histogram reweighting technique is complementary to the use of improved estimators. It is a quite general technique of data analysis based on the simple idea of recording whole distribution functions, and not only their first few moments (e.g., the average energy and specific heat), as is usually done. The energy distribution $\mathcal{P}_{\beta_0}(E)$ (normalized to unit area) at inverse temperature β_0 can be written as

$$\mathcal{P}_{\beta_0}(E) = \rho(E)e^{-\beta_0 E}/Z(\beta_0) , \tag{9}$$

where $\rho(E)$ is the density of states with energy E. It is then easy to see that an expectation value $\langle f(E)\rangle$ can in principle be calculated for any β from

$$\langle f(E)\rangle(\beta) = \frac{\int_0^\infty dE\, f(E)\mathcal{P}_{\beta_0}(E)e^{-(\beta-\beta_0)E}}{\int_0^\infty dE\, \mathcal{P}_{\beta_0}(E)e^{-(\beta-\beta_0)E}} . \tag{10}$$

To keep the notation short, we have suppressed the lattice-size dependence of $\mathcal{P}_{\beta_0}(E)$.

In practice, the continuous energy has to be discretized into bins of size ΔE, and one measures the associated histogram $P_{\beta_0}(E) = \mathcal{P}_{\beta_0}(E)\Delta E$. Since the wings of $P_{\beta_0}(E)$ have large statistical errors, one expects Eq. (10) (or its obvious discrete modification) to give reliable results only for β near β_0. If β_0 is near criticality, the distribution is relatively broad and the method works best. In this case reliable estimates from (10) can be expected for β values in an interval around β_0 of width $\propto L^{-1/\nu}$, i.e., just in the FSS region. Figure 1(a) shows three typical energy histograms measured at slightly different temperatures near the critical point for the lattice size $L=48$.

The information stored in $P_{\beta_0}(E)$ is not yet sufficient to calculate also the magnetic moments $\langle m^k\rangle(\beta)$ with $m=|\mathbf{m}|$ as function of β from a single simulation at β_0. Conceptually, the simplest way to do so is to record the two-dimensional histogram $P_{\beta_0}(E,M)$, where $M=mV$ is the total magnetization (in general, we will denote by lowercase letters quantities per site and the associated total quantities by the corresponding capital letters). Since disk space limitations prevented us from doing that,[33] we have measured instead the "microcanonical averages"

$$\langle\langle m^k\rangle\rangle(E) = \sum_M P_{\beta_0}(E,M)m^k/P_{\beta_0}(E) , \tag{11}$$

where we have used the trivial relation $\sum_M P_{\beta_0}(E,M) = P_{\beta_0}(E)$. In practice, this can be done simply by accumulating the measurements of m^k in different slots or bins according to the energy of the configuration and normalizing at the end by the total number of hits of each energy bin. Clearly, once $\langle\langle m^k\rangle\rangle(E)$ is determined, this is a special case of $f(E)$ in Eq. (10), so that

$$\langle m^k\rangle(\beta)=\frac{\sum_E \langle\langle m^k\rangle\rangle(E)P_{\beta_0}(E)e^{-(\beta-\beta_0)E}}{\sum_E P_{\beta_0}(E)e^{-(\beta-\beta_0)E}} . \quad (12)$$

Similar to $\rho(E)$ in (9), theoretically the microcanonical averages $\langle\langle m^k\rangle\rangle(E)$ do not depend on the temperature at which the simulation is performed. Because of the limited statistics in the wings of $P_{\beta_0}(E)$, however, there is only a finite range around $E_0\equiv\langle E\rangle(\beta_0)$ where one can expect reasonable results for $\langle\langle m^k\rangle\rangle(E)$. Outside of this range it simply can happen (and does happen) that there are no events to be averaged. This is illustrated in Fig. 1(b),

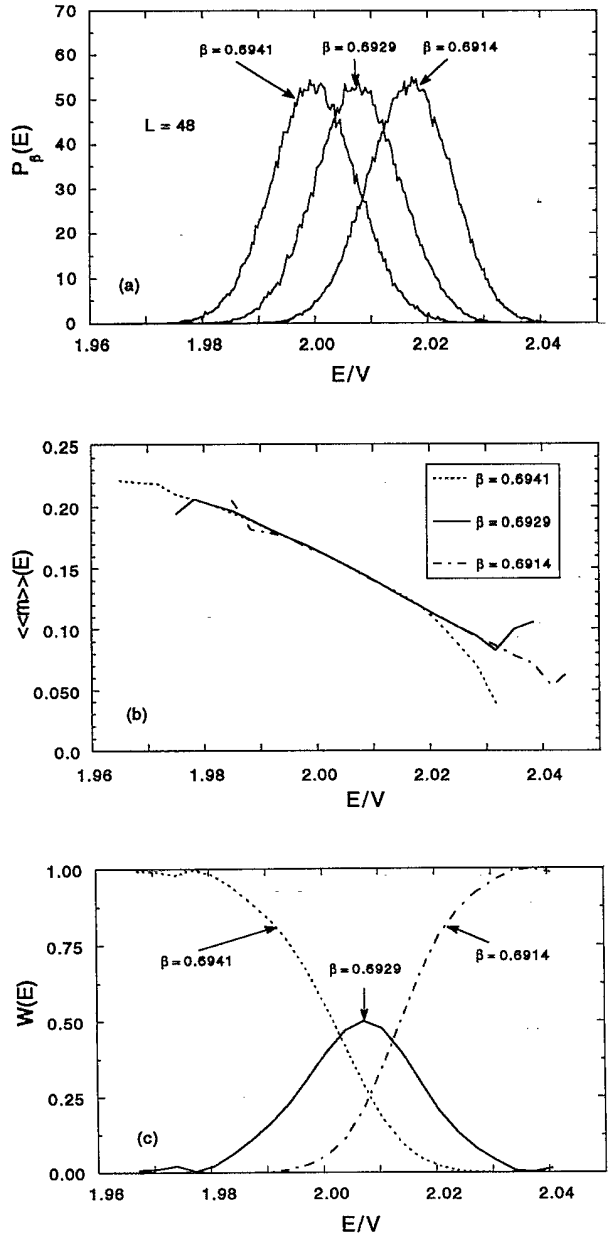

FIG. 1. (a) Energy histograms for $L=48$ at the three simulation temperatures. (b) The constant energy averages $\langle\langle m\rangle\rangle(E)$ as computed from the three simulations yielding the histograms in (a). (c) The weights for the optimal combination of the histograms according to the procedure in Ref. 27.

where $\langle\langle m\rangle\rangle(E)$ is plotted versus energy as obtained from the three runs which gave the energy histograms in Fig. 1(a). We see that the function looks smooth only in the range where the corresponding energy histogram in Fig. 1(a) has enough statistics.

To take full advantage of the histogram reweighting technique, we have performed for each L typically three[34] simulations at slightly different inverse temperatures β_i. Using histogram reweighting and jackknife blocking,[35] we computed the β dependence of the expectation values for all interesting thermodynamic observables $O_i \equiv O_L^{(\beta_i)}(\beta)$ plus the associated error ΔO_i. To obtain a single expression $O\equiv O_L(\beta)$, we then combined the values O_i numerically according to the formula

$$O=\left[\frac{O_1}{(\Delta O_1)^2}+\frac{O_2}{(\Delta O_2)^2}+\frac{O_3}{(\Delta O_3)^2}\right](\Delta O)^2 , \quad (13)$$

where ΔO is given by

$$\frac{1}{(\Delta O)^2}=\frac{1}{(\Delta O_1)^2}+\frac{1}{(\Delta O_2)^2}+\frac{1}{(\Delta O_3)^2} . \quad (14)$$

This expression minimizes the absolute error ΔO. The reweighting range of each simulation, i.e., that range in which the energy histogram has enough statistics to allow for (10) to be valid, was determined by the energy values at which the histogram had decreased to a third of its maximum value.[36] From the energy range one can then deduce a corresponding β range. Only the values inside this β window were used for the optimized combination (13); the contributions of the other values were suppressed by giving them zero weights.

We also implemented the optimized histogram combination discussed in Ref. 27 to cross-check the results obtained by (13) for the specific heat. The Fig. 1(c) shows the weights for the optimal combination of the primary energy histograms according to the prescription of Ref. 27, i.e., which gives the optimal combination of the three estimates for $N(E)\equiv\rho(E)\Delta E$. Both methods gave comparable results within the statistical errors. We preferred our optimization procedure over the optimized histogram addition because it is simpler to apply to quantities involving constant energy averages such as $\langle\langle m\rangle\rangle(E)$ and, more importantly, minimizes the error on each observable of interest separately.

III. RESULTS AT CRITICALITY AND FINITE-SIZE SCALING ANALYSIS

We investigated in our MC study simple cubic lattices of volume $V=L^3$, where $L=12$, 16, 20, 24, 32, 40, and 48. For each L we have made at least three simulations at three different temperatures compiled in Table I. For all L we took $\beta=0.6929$, because this is the critical inverse temperature found in the recent study of Peczak, Ferrenberg, and Landau.[23] We analyzed this run to locate a first estimate for the temperatures of the maxima of the specific heat and the susceptibility for each L, and used those two temperatures for our other two simulations. This choice has the advantage that both locations of the maxima scale approximately like $L^{-1/\nu}$, which is

also the region after which the energy distribution $P_\beta(E)$ has decreased by roughly the same factor for all L. We can therefore expect to have always enough overlap to ensure a safe reweighting of our three histograms into the β region of interest. A further advantage is that the two maxima approach T_c from different sides.

For each configuration we recorded the energy histogram $P_\beta(E)$ using 90 000 bins to discretize the continuous energy range $0 \le E \le 3V$. We have checked that this binning is fine enough to ensure negligibly small discretization errors. In addition, we recorded the microcanonical averages of $\langle\langle m \rangle\rangle(E)$, $\langle\langle m^2 \rangle\rangle(E)$, and $\langle\langle m^4 \rangle\rangle(E)$. These histograms provided us with all necessary information to calculate all thermodynamic quantities of interest. Every 10 000 measurement steps we recorded a copy of each histogram, so that we were able to compute errors by standard jackknife blocking.[35]

A. Binder parameter $U_L(\beta)$

We have used the histogram reweighting technique to find the β dependence of the Binder parameter,[37]

$$U_L(\beta) = 1 - \frac{1}{3}\frac{\langle m^4 \rangle}{\langle m^2 \rangle^2} . \tag{15}$$

To obtain a single curve $U_L(\beta)$ for each lattice size L from the three simulations at temperatures compiled in Table I, we used our optimized combination of Eq. (13). In (15) we adapt the usual normalization convention, although the factor 3 is only really motivated for the Ising [$O(1)$] model. For general $O(n)$ models it is easy to show that in the high-temperature limit Gaussian fluctuations around $\mathbf{m}=0$ lead to $U_L \to 2(n-1)/3n$. For $n=1$ this gives a zero reference point, but for the Heisenberg model with $n=3$ we get the quite arbitrary looking limit $U_L \to \frac{4}{9}$. In three dimensions we are for low temperatures always in the magnetized phase and hence have for all n trivially $U_L \to \frac{2}{3}$.

It is well known[37] that the $U_L(\beta)$ curves for different L cross around (β_c, U^*) with slopes $\propto L^{1/\nu}$, apart from confluent corrections explaining small systematic deviations. This allows an almost unbiased estimate of β_c, the critical exponent ν, and U^*. Field-theoretical expansions in $\sqrt{\varepsilon} \equiv \sqrt{4-D}$ predict[38]

$$U^* = 0.59684\ldots . \tag{16}$$

This follows from the expansion

$$\begin{aligned}\frac{\langle m^4 \rangle}{\langle m^2 \rangle^2} &= \frac{3}{4}\frac{\Gamma^2(\frac{3}{4})}{\Gamma^2(\frac{5}{4})}\left[1 - x_0\sqrt{6}\left[\frac{\Gamma(\frac{9}{4})}{\Gamma(\frac{7}{4})} + \frac{\Gamma(\frac{5}{4})}{\Gamma(\frac{3}{4})} - 2\frac{\Gamma(\frac{7}{4})}{\Gamma(\frac{5}{4})}\right]\right. \\ &\quad \left. + 6x_0^2\left[\frac{\Gamma(\frac{9}{4})\Gamma(\frac{5}{4})}{\Gamma(\frac{7}{4})\Gamma(\frac{3}{4})} + 3\frac{\Gamma^2(\frac{7}{4})}{\Gamma^2(\frac{5}{4})} - 4\right]\right] \\ &= \frac{12}{R^2}\left[1 - x_0\sqrt{6}\left[\frac{2}{3}R - \frac{6}{R}\right]\right. \\ &\quad \left. + 6x_0^2\left[\frac{5}{48}R^2 + \frac{27}{R^2} - 4\right]\right] , \end{aligned} \tag{17}$$

where

$$x_0 = -1.765\,084\,801\,2\frac{5}{2\sqrt{33}}\sqrt{\varepsilon} = -0.768\,154\,56\sqrt{\varepsilon} ,$$

and in the last line we have abbreviated $R \equiv \Gamma(\frac{1}{4})/\Gamma(\frac{3}{4}) = 2.958\,675\,12\ldots$. Note also that (15) can be rewritten as

$$U_L = \frac{2}{3} - \frac{\sigma_\chi^2}{3\chi^2} , \tag{18}$$

where $\sigma_\chi^2 \equiv V^2\beta^2(\langle m^4 \rangle - \langle m^2 \rangle^2)$ is the variance of the susceptibility. In the $T \to \infty$ limit, we get $\sigma_\chi^2 \to \frac{2}{3}\chi^2$ and at criticality, inserting the field-theory prediction (16), this implies $\sigma_\chi^2 \approx 0.21\chi^2$.

Figure 2 shows the crossings of the $U_L(\beta)$ curves on a large scale, which gives a first estimate of (β_c, U^*). To extract more precise values of U^* and β_c from our data, we used that the locations of the crossing point $\beta^\times \equiv 1/T^\times$ of two different curves $U_L(\beta)$ and $U_{L'}(\beta)$ depend on the scale factor $b = L'/L$, as a result of the residual corrections to the FSS.[37] To have enough data points for a straight-line fit, we used only the crossing points of the $L=12$ and 16 curves with all the other ones with higher L' value, which gave us six and five data points, respectively. The two least-squares extrapolations in the plot of $T^\times$ vs $1/\log_{10} b$ shown in Fig. 3 are consistent with each other and gave us the values $\beta_c = 0.69297(9)$ and 0.69298(13), respectively. Combining the two values, we

$$\beta_c = 0.6930 \pm 0.0001 . \tag{19}$$

The errors obtained on $T^\times$ were obtained by using the crossings of $U_L(\beta) + \Delta U_L(\beta)$ with $U_{L'}(\beta) - \Delta U_{L'}(\beta)$, where ΔU_L are the errors on U_L obtained via the jackknife procedure. Our result (19) is in good agreement with the value given in Ref. 23, $\beta_c = 0.6929(1)$, but significantly higher than estimates from analyses of high-temperature series expansions.[39,40]

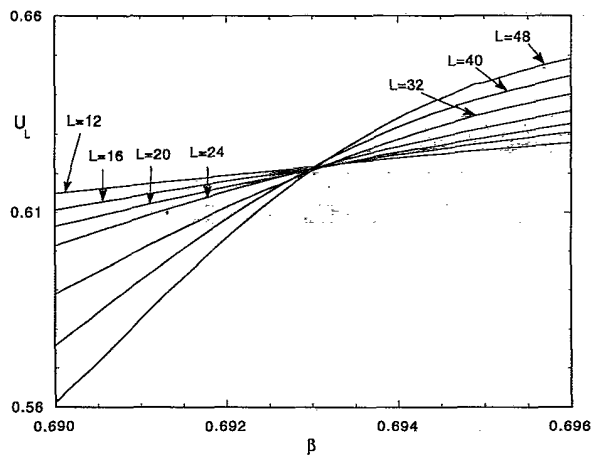

FIG. 2. Binder parameter U_L vs β. The values of $U_L(\beta)$ were obtained by reweighting and optimized combining the results of our three simulations at different temperatures for each lattice size L. The simulations were performed at $\beta_0 = 0.6929$ [the critical inverse temperature found by Peczak, Ferrenberg, and Landau (Ref. 23)] and at the positions of the maxima of the specific heat C and the susceptibility χ^c, respectively.

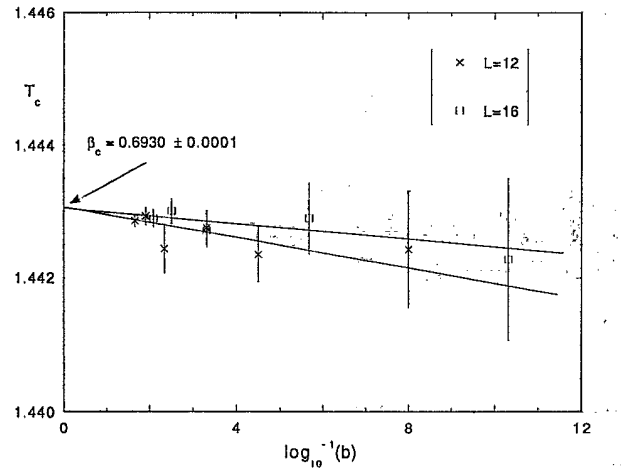

FIG. 3. Estimates for T_c, coming from plotting the T values of the crossing points of the $L=12$ and 16 curves of the Binder parameter U_L vs the inverse logarithm of the scale factor $b=L'/L$. The extrapolation leads to an estimate of $\beta_c=0.6930(1)$.

A similar analysis[37] was used to determine U^*, which resulted in $U^*=0.62175(35)$ and 0.62141(75), respectively, from which we extract the final estimate

$$U^*=0.6217\pm0.0008\ . \tag{20}$$

The theoretical prediction (16) based on the $\sqrt{\varepsilon}$ expansion is about 4% smaller than this value. The deviation is somewhat less than for the XY model where it is about 6%.[17,18]

To determine the derivative $dU_L/d\beta$, we first used a finite-difference approximation at our estimate of β_c. But we observed that the results depended very sensitively on the interval of the linear approximation and on the kind of finite-difference derivative used, i.e., backward, forward, or symmetric derivative. We have therefore chosen another method[41] to calculate the slope of $U_L(\beta)$ that is less sensitive to systematic errors. We took the thermodynamic derivative of U_L with respect to β, which can be written as

$$\frac{dU_L}{d\beta}=\frac{1}{3\langle m^2\rangle^2}\left\{\langle m^4\rangle\langle E\rangle - 2\frac{\langle m^4\rangle\langle m^2E\rangle}{\langle m^2\rangle}+\langle m^4E\rangle\right\}$$
$$=(1-U_L)\left\{\langle E\rangle-2\frac{\langle m^2E\rangle}{\langle m^2\rangle}+\frac{\langle m^4E\rangle}{\langle m^4\rangle}\right\}. \tag{21}$$

The expectation values for $\langle m^kE\rangle(\beta)$ at temperature β can be calculated from

$$\langle m^kE\rangle(\beta)=\frac{\sum_E E\langle\langle m^k\rangle\rangle(E)P_{\beta_0}(E)e^{-(\beta-\beta_0)E}}{\sum_E P_{\beta_0}(E)e^{-(\beta-\beta_0)E}}, \tag{22}$$

generalizing Eq. (10). For each L and β, we obtained in this way three estimates of $(dU_L/d\beta)(\beta)$ that we combined optimally according to the errors of $dU_L/d\beta$.

In Fig. 4 we plot $(dU_L/d\beta)(\beta_c)$, taken at our estimate of $\beta_c=0.6930$, versus L on a log-log scale. From the inverse slope we read off

$$\nu=0.704\pm0.006\ , \tag{23}$$

with a quality factor $Q=0.61$, relying on the linear least-squares-fit routine FIT of Ref. 42. For comparison, the field-theoretical estimates are $\nu=0.705(3)$ (resummed perturbation series[43]), $\nu=0.710(7)$ (resummed ε expansion[44]). We noted that the value of ν derived in this way was strongly dependent on the temperature at which it was extracted. It turned out that the systematic errors one gets by choosing a slightly different value for β_c are larger than the statistical errors. The strong β dependence of $dU_L/d\beta$ has its origin in the large system sizes we used that make the thermodynamic quantities vary very rapidly with β. For comparison, for $\beta=0.6929$ ($\beta=0.6931$) we obtained $\nu=0.696(6)$ with $Q=0.76$ [$\nu=0.712(6)$ with $Q=0.49$] (see also Fig. 8 below). An alternative method would have been to look at the scaling of the maxima of the slope of U_L, which would require no knowledge of β_c. Unfortunately, it turned out that the maxima occur too far on the high-temperature side and lie outside of the reliable reweighting range.

B. Magnetization and susceptibility

To extract the ratio of critical exponents β/ν, we used that the magnetization at β_c should scale for sufficiently large L like[3]

$$\langle m\rangle\propto L^{-\beta/\nu}\ . \tag{24}$$

The slope of the straight line in the log-log plot shown in Fig. 5 of $\langle m\rangle$ vs L at $\beta_c=0.6930$ gives a value of

$$\beta/\nu=0.514\pm0.001\ , \tag{25}$$

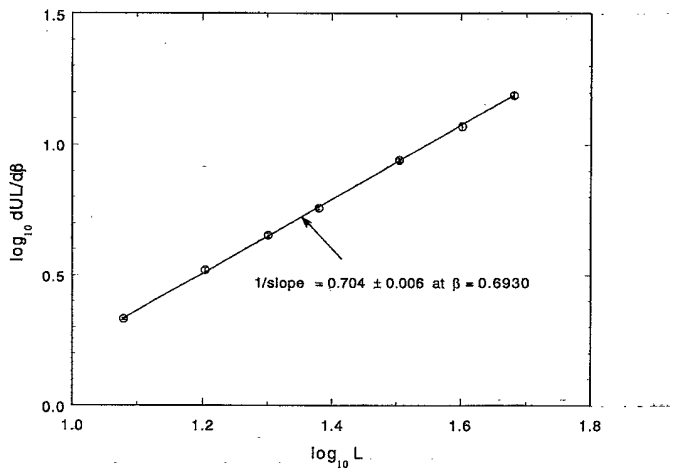

FIG. 4. Thermodynamic derivative $dU_L/d\beta$ calculated at $\beta_c=0.6930$ vs lattice size L in a double-logarithmic plot. The slope of the linear least-squares fit gives an estimate for the critical exponent of the correlation length, $\nu=0.704(6)$, with a quality $Q=0.61$.

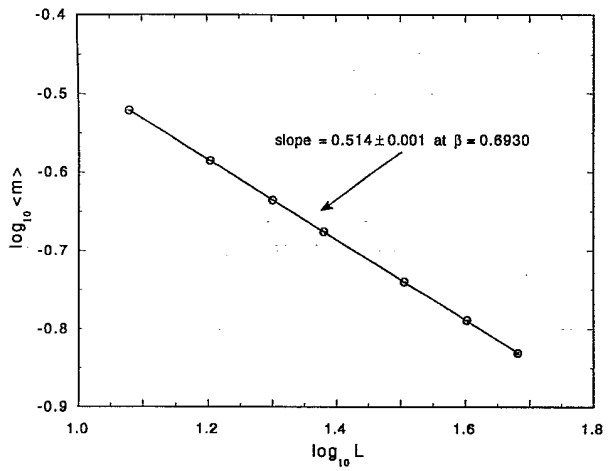

FIG. 5. Double-logarithmic plot of the magnetization $\langle m \rangle$ at $\beta_c = 0.6930$ vs lattice size L. The values of $\langle m \rangle$ were obtained by reweighting and optimized combining (see text) of our three simulations at different temperatures for each lattice size L. The slope gives an estimate for β/ν. From the fit we obtain $\beta/\nu = 0.514(1)$, with quality $Q = 0.68$.

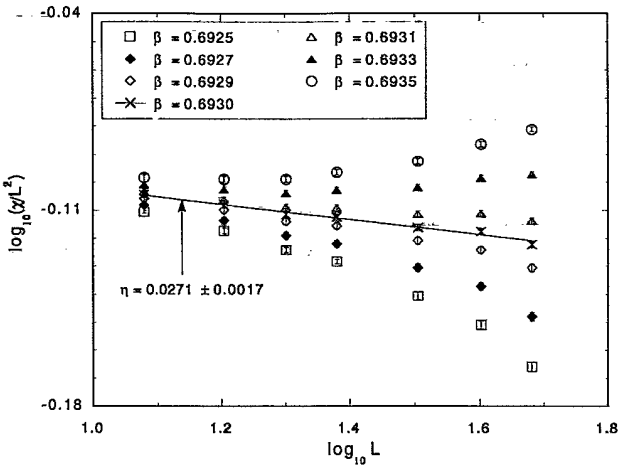

FIG. 6. $\log_{10}(\chi/L^2)$ vs $\log_{10}(L)$ at inverse temperatures $\beta = 0.6925$ (□), $\beta = 0.6927$ (◆), $\beta = 0.6929$ (◇), $\beta = 0.6930$ (×), $\beta = 0.6931$ (△), $\beta = 0.6933$ (▲), and $\beta = 0.6935$ (○). The straight line corresponds to a linear least-squares fit at $\beta = 0.6930$, which gives $\eta = 0.0271(17)$ with $Q = 0.78$.

with a Q value of 0.68 of our linear least-squares fit routine. We noted again that the systematic error of choosing an incorrect β_c was larger than the statistical error coming from the fit. For example, for fits of $\langle m \rangle$ at the two inverse temperatures $\beta = 0.6929$ and 0.6931, we obtained $\beta/\nu = 0.519(1)$ and 0.509(1) with values $Q = 0.30$ and 0.31, respectively. We take the significant lower Q values as supporting our estimate of β_c (compare also Fig. 8 and the discussion of the Q values later in this section). Using our estimate of $\nu = 0.704(6)$, we get for the critical exponent of the magnetization $\beta = 0.362(4)$.

On finite lattices an estimator for the magnetic susceptibility per spin is given by

$$\chi^c = V\beta(\langle m^2 \rangle - \langle m \rangle^2) , \tag{26}$$

where the superscript c stands for "connected." In the high-temperature phase the true magnetization vanishes, $\langle \mathbf{m} \rangle = 0$, and one may also use

$$\chi = V\beta\langle m^2 \rangle \quad \text{for } \beta < \beta_c . \tag{27}$$

Since both expressions should scale at criticality like $L^{\gamma/\nu} = L^{2-\eta}$, a straight-line fit in a double-logarithmic plot of χ/L^2 vs L gives an estimate of η. We preferred to visualize η as opposed to γ/ν because η is the more sensitive parameter. The results for different choices of β_c are shown in Fig. 6. We see that our estimate of β_c in (19) seems to be very reasonable, which is also supported by the fact that it results in the fit with the highest Q value. The fact that the curves with $\beta > \beta_c$ ($\beta < \beta_c$) bend upwards (downwards) is easily understood by recalling that in the low-temperature phase χ scales with the volume $V = L^3$, while in the high-temperature phase χ eventually saturates at a finite value for any L. Close to criticality, as long as the scaling variable $x \equiv (1-\beta/\beta_c)L^{1/\nu}$ satisfies $|x| \ll 1$ and $L \gg 1$, we expect from FSS that the deviations from $-\eta \log_{10} L + c_0$ should be simply given by $c_1 x$, where c_0 and c_1 are approximately constant (apart from small confluent corrections $\propto L^{-\omega}$). For all data points in Fig. 6, we have $|x| < 0.18$ and the linear scaling with $(1-\beta/\beta_c)$ is obviously satisfied. Moreover, a closer look shows that also the scaling with $L^{1/\nu}$ is very well confirmed (using our estimate of $\nu = 0.704$ the deviations from the straight-line fit of the curves at $\beta \neq \beta_c$ for $L = 32$, 40, and 48 should be stronger than those for $L = 24$ by factors of about 1.5, 2.1, and 2.7, respectively). In fact, in a scaling plot all curves would fall on top of each other. The theoretical predictions for η are 0.040(3) (resummed ε expansion) and 0.033(4) (resummed perturbation series), and inserting (25) in the scaling relation $\eta = 2\beta/\nu - 1$ gives $\eta = 0.028(2)$. Our direct estimates of η for $\beta = 0.6930 \pm 0.0001$ are collected in Table II. It is also interesting to note that η gets closer to the theoretical values for $\beta < \beta_c$ for χ and for $\beta > \beta_c$ for χ^c, hence just in the regions in which both expressions are naturally used. Another check on η can be obtained from the maxima of χ^c, which should obey the same scaling law as χ^c and χ at β_c. The results are compiled in Table II. Our three estimates for η barely agree in the 2σ range, but this is mainly due to the low estimate of η coming from the χ^c fit. This behavior of the χ^c scaling law is in agreement with the findings of Refs. 23 and 45, wherein it was also observed that the χ^c fit results in a noticeably lower η value. As our final estimate, we take the result from the best fit of χ at $\beta_c = 0.6930$, yielding

$$\eta = 0.0271 \pm 0.0017 . \tag{28}$$

This in turn implies $\gamma/\nu = 2 - \eta = 1.9729(17)$ and, using again our value of ν, $\gamma = 1.389(14)$.

From the temperature locations $T_{\chi^c_{\max}}$ of the (connected) susceptibility maxima, one can get another estimate of β_c by using the scaling prediction $T_{\chi^c_{\max}}$

TABLE II. Results for η obtained from log-log fits of χ/L^2 and χ^c/L^2 vs the lattice size L at three temperatures near β_c. Included is also the estimate of η coming from a fit of the maximum $\chi^c_{\max}$ of the connected susceptibility (see text). Q denotes the quality factor of the least-squares-fit routine FIT of Ref. 42.

	χ		χ^c		$\chi^c_{\max}$	
β	η	Q	η	Q	η	Q
0.6929	0.0364(17)	0.36	0.0086(44)	0.71	0.0231(61)	0.30
0.6930	0.0271(17)	0.78	0.0156(44)	0.69		
0.6931	0.0178(17)	0.43	0.0237(44)	0.48		

$=T_c+aL^{-1/\nu}+\cdots$. Using our previously determined value of $\nu=0.704$, we get from the linear fit shown in Fig. 7 the estimate $\beta_c=0.6930(3)$, with $Q=1$, which is in excellent agreement with our result (19) for β_c obtained from the U_L crossing points. The data for the fit is compiled in Table III.

When we did our least-squares fitting of quantities extracted at a particular β, we noticed that the Q value can also be used as a very sensitive measure to obtain an estimate of the critical temperature, whose error is comparable to the one obtained from the fits to the U_L crossing points. Obviously, if one extracts data at temperatures away from β_c, the subleading corrections to the scaling laws become more important and worsen the fit substantially, especially if large lattices are used. In Fig. 8 we plot the quality factor Q obtained from log-log linear least-squares fits of the quantities $(dU_L/d\beta)(\beta)$, $\langle m\rangle(\beta)$, $\chi(\beta)$, and $\chi^c(\beta)$ versus the lattice size L, extracted at different inverse temperatures. The most striking results come from the $Q(\beta)$ curves of $\langle m\rangle$ and χ, which seem to have the most severe β dependence. Their peak locations are exactly at $\beta=0.6930$ with an estimated error of ± 0.0001, whereas the $Q(\beta)$ curves of $(dU_L/d\beta)(\beta)$ and $\chi^c(\beta)$ do not peak so sharply at some β and are asymmetric with respect to their peak location, falling off very slowly on the high-temperature side. The slow variation of the Q value of the $(dU_L/d\beta)(\beta)$ fits indicates that

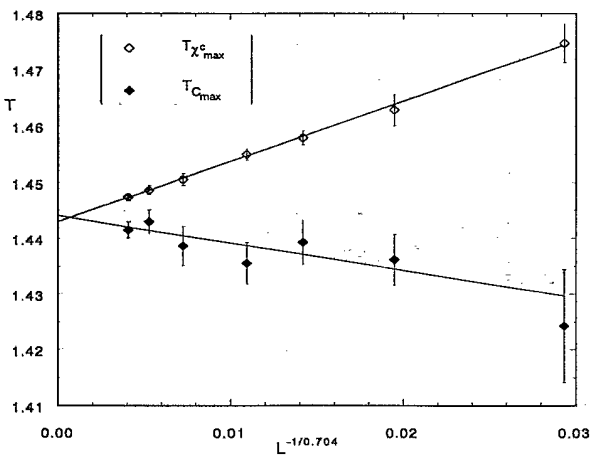

FIG. 7. Variation of the pseudotransition temperatures $T_{\chi^c_{\max}}(L)$ and $T_{C_{\max}}(L)$ with $L^{-1/\nu}$, where $\nu=0.704(6)$ is our estimate obtained in Fig. 4. The fits yield estimates of $\beta_c=0.6930(3)$ ($Q=1.0$) and $\beta_c=0.6925(9)$ ($Q=0.80$), respectively.

Binder's method to determine ν is less sensitive to the choice of β_c than the FSS method for β/ν and γ/ν, as is expected on theoretical grounds.[37] This is reflected in our data for ν, where the systematic errors for different choices of the critical coupling are of the order of the statistical errors, whereas for β/ν they are 5 times as big.

C. Energy and specific heat

Assuming hyperscaling, $\alpha=2-D\nu$, to be valid and inserting our estimate $\nu=0.704(6)$, we get a negative value for the critical exponent of the specific heat, $\alpha=-0.112(18)$. This implies a cusplike singularity at T_c, but no divergence at all. Although at first sight this sounds numerically very convenient, it turns out that the specific heat is the hardest observable to analyze. On the one hand, it is quite easy to get the peak height with good precision because of the smoothness of the specific heat. On the other hand, however, the scaling behavior is quite unclear for $\alpha<0$, since one has to deal with large, nonuniversal background terms. For the peak location $T_{C_{\max}}(L)$, the scaling behavior is of the usual form $T_{C_{\max}}(L)\approx T_C+aL^{-1/\nu}$, but now the smoothness of the peaks makes it numerically difficult to determine $T_{C_{\max}}(L)$ with high precision.

We calculated the specific heat in two different ways, once from the energy fluctuations as

$$C=V\beta^2(\langle e^2\rangle-\langle e\rangle^2) \tag{29}$$

and the other time as a finite-difference derivative approximating $C=de/dT$. Both definitions resulted in similar curves, and this time the choice of the finite-difference scheme did not affect the results. Because the curves of definition (29) were smoother in appearance, we decided to use solely the first definition to extract our scaling information. The maximum of the specific heat should scale as

$$C_{\max}(L)\approx C^{\rm reg}_{\max}-aL^{\alpha/\nu}, \tag{30}$$

where $C^{\rm reg}_{\max}$ is a regular background term. Using the routine MRQMIN of Ref. 42, we obtained from a three-parameter fit the values $C^{\rm reg}_{\max}=4.17(97)$, $a=3.98(17)$, $\alpha/\nu=-0.33(22)$, with a Q value of $Q=0.69$. Using our estimate of $\nu=0.704(6)$, this results in $\alpha=-0.23(16)$. This estimate is clearly larger than the one obtained through hyperscaling, but, because of its large error bar, it is still consistent. By imposing the hyperscaling value of $\alpha/\nu=2/\nu-3=-0.159$, we also did a linear fit of

TABLE III. Data for the temperature locations and the absolute values of the maxima of the magnetic susceptibility and the specific heat. The data were extracted from the optimally combined curve of the three runs for each lattice size (compare text).

L	$T_{\chi^c_{\max}}$	$\chi^c_{\max}$	$T_{C_{\max}}$	$C_{\max}$
12	1.4747(35)	5.260(38)	1.4243(101)	2.426(11)
16	1.4629(28)	9.242(100)	1.4362(45)	2.579(26)
20	1.4579(13)	14.25(10)	1.4393(39)	2.711(20)
24	1.4550(11)	20.80(09)	1.4355(37)	2.778(15)
32	1.4505(11)	36.53(22)	1.4386(35)	2.936(34)
40	1.4486(08)	56.45(39)	1.4430(21)	2.959(46)
48	1.4474(06)	81.48(63)	1.4415(15)	3.090(50)

$C_{\max}(L)$ vs $L^{\alpha/\nu}$ that gave us $C^{\text{reg}}_{\max}=5.79(12)$ and $a=5.00(19)$ with $Q=0.71$. Both curves fit the data almost equally good, as can be inspected in Fig. 9.

The fit of $T_{C_{\max}}(L)$ vs $L^{-1/\nu}$ is shown in Fig. 7. Assuming $\nu=0.704$, our linear-fit routine gave $\beta_c=0.6925(9)$ with $Q=0.80$. Because of the large error bars on $T_{C_{\max}}$, this estimate has the largest statistical scatter, but is still in agreement with our previous estimates of β_c. The data for the fit can be found in Table III.

IV. RESULTS IN THE HIGH-TEMPERATURE PHASE

Let us now turn to the analysis of our second set of simulations, which were performed in the high-temperature phase. Here we have mainly concentrated on measurements of the spatial correlation length ξ and the susceptibility $\bar{\chi}$ using the improved estimators of Sec. II B. From least-squares fits to the critical divergencies of ξ and $\bar{\chi}$ as function of T or β, we can get independent estimates of the critical coupling β_c and of the critical exponents ν and γ. This of course requires us to keep finite-size corrections as small as possible. We therefore have chosen the linear size of the lattices to satisfy the condition $L \geq 8\xi$, which proved in related studies[11,12] to be a safe condition. In a few cases we have checked this once again by performing test runs at smaller $L \approx 5-7\xi$. As a result, to avoid the most severe finite-size corrections, also for this model it would probably be sufficient to choose $L \approx 6\xi$.

Our final data set consists of 18 points between $\beta=0.650$ and 0.686 (corresponding to correlation lengths $\xi=3,\ldots,12$; see below) using lattices of sizes between 32^3 and 100^3. The simulation parameters together with the statistics and the results are compiled in Table IV. The statistics is given in terms of N, the number of measurements of the standard estimators which, on the average, were taken after $f\times V$ spins are flipped. The number of Metropolis equivalent sweeps is then simply $f\times N$. The average cluster size $\langle |C| \rangle$ is given in terms of the ratio $\langle |C| \rangle / \bar{\chi}_{\text{imp}}$, which is only very slowly varying over a wide temperature range. The column labeled with C shows the specific heat calculated from the energy fluctuations. For comparison we give for the susceptibility the averages over standard as well as over improved estimators. We see that the errors on $\bar{\chi}_{\text{imp}}$ are smaller by about a factor of 2–3. It should be mentioned that the errors on $\bar{\chi}$ could be somewhat reduced by doing measurements more frequently (i.e., by choosing smaller

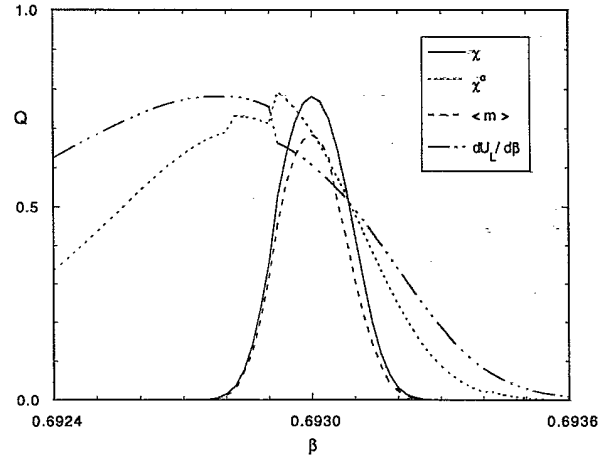

FIG. 8. Q value (quality factor) of linear least-squares log-log fits of the quantities $\chi(\beta)$, $\chi^c(\beta)$, $\langle m \rangle(\beta)$, and $(dU_L/d\beta)(\beta)$ vs the lattice size L, extracted at different β values in intervals of $\Delta\beta=0.000\,02$.

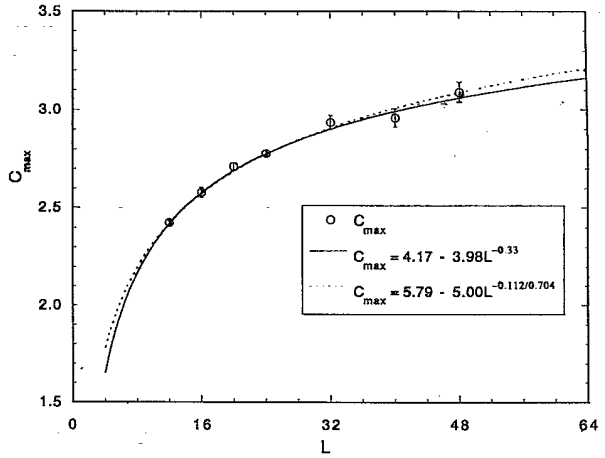

FIG. 9. Lattice-size dependence of the maxima of the specific heat, $C_{\max}$. The solid curve is a nonlinear three-parameter fit, whereas the dashed curve comes from a linear fit with fixed $\alpha/\nu=2/\nu-D=-0.159$, employing hyperscaling arguments and our estimate of $\nu=0.704(6)$.

TABLE IV. Results in the high-temperature phase. N is the number of measurements of the nonimproved observables, taken after $f \times L^3$ spins are flipped (on the average). C denotes the specific heat, and $\langle |C| \rangle$ is the average cluster size. The cluster size and the improved observables are measured after each cluster-update step.

β	L	$L/\xi_{\rm imp}$	$N/10^3$	f	$\langle \lvert C \rvert \rangle / \bar{\chi}_{\rm imp}$	C	$\bar{\chi}$	$\bar{\chi}_{\rm imp}$	$\xi_{\rm imp}$
0.650	32	9.9	79.5	0.270	0.7556	1.074(13)	46.00(15)	45.697(50)	3.2345(26)
0.655	32	9.0	263.6	0.134	0.7547	1.137(11)	54.43(12)	54.280(53)	3.5412(24)
0.660	32	8.1	93.0	0.271	0.7539	1.222(13)	65.95(21)	66.095(89)	3.9336(34)
0.665	40	9.0	400.0	0.133	0.7531	1.310(11)	83.07(14)	83.155(65)	4.4343(24)
0.670	40	7.8	138.8	0.134	0.7523	1.382(19)	109.32(33)	109.59(18)	5.1260(53)
0.673	50	8.8	89.5	0.133	0.7519	1.453(23)	132.77(47)	132.76(22)	5.6676(62)
0.675	50	8.2	114.4	0.132	0.7517	1.470(24)	153.92(48)	153.99(26)	6.1197(64)
0.676	60	9.4	132.3	0.133	0.7515	1.539(21)	167.07(47)	166.69(21)	6.3740(55)
0.677	60	9.0	68.5	0.133	0.7515	1.560(29)	181.71(72)	181.16(34)	6.6584(83)
0.678	60	8.6	170.5	0.133	0.7513	1.562(20)	198.52(49)	198.74(25)	6.9869(58)
0.679	60	8.2	156.3	0.133	0.7512	1.619(21)	218.82(58)	218.46(32)	7.3333(68)
0.680	60	7.8	95.3	0.162	0.7511	1.700(28)	242.04(79)	242.17(44)	7.7359(87)
0.681	70	8.5	295.5	0.133	0.7510	1.710(17)	270.68(51)	270.96(27)	8.2013(52)
0.682	70	8.0	154.9	0.133	0.7508	1.776(23)	304.38(79)	305.91(46)	8.7244(81)
0.683	80	8.6	73.4	0.157	0.7508	1.765(31)	348.5(1.3)	349.26(63)	9.346(11)
0.684	80	7.9	138.4	0.133	0.7506	1.778(25)	405.9(1.2)	405.92(62)	10.0988(94)
0.685	90	8.2	174.0	0.133	0.7505	1.903(24)	477.9(1.2)	478.60(64)	10.9857(92)
0.686	100	8.3	77.4	0.133	0.7504	1.860(36)	575.0(2.0)	576.9(1.1)	12.093(15)

values of f). The reason is that the (integrated) autocorrelation time for $\bar{\chi}$ is still very small on the time scale at which the measurements are taken (≈ 0.8, translating in Metropolis equivalent units to $0.8f \approx 0.1$). On the other hand, it should be kept in mind that each standard measurement takes $\mathcal{O}(V)$ operations, so that too small a factor f would slow down the simulation considerably. The correlation length in the last column was extracted from fits to the inverse Fourier transform of the spatial correlation function as described in Sec. II B. We always used the lattice momentum squared, $\sum_{i=1}^{3} 2(1-\cos k_i)$, $k_i = (2\pi/L)n_i$, as an independent variable. In Fig. 10 this procedure is illustrated for our largest lattice of size 100^3. We have checked that within error bars the estimates for

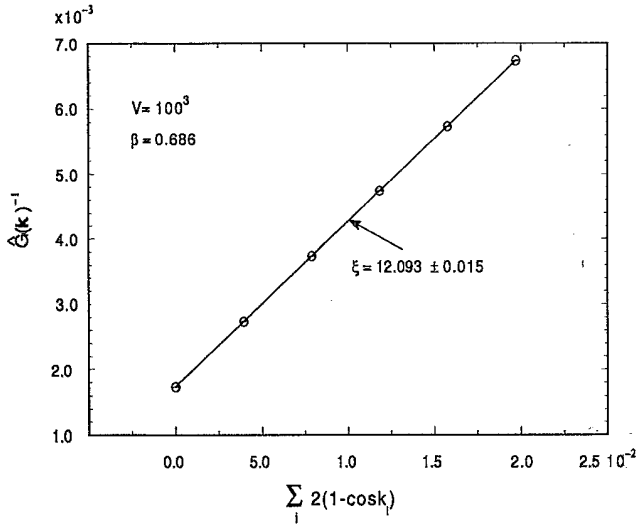

FIG. 10. Fit of $\hat{G}(\mathbf{k})^{-1}$ to $c[\sum_{i=1}^{3} 2(1-\cos k_i) + (1/\xi)^2]$ on a 100^3 lattice used to compute the correlation length ξ.

$\xi_{\rm imp}$ do not depend on how many Fourier coefficients we use in the fits. This observation is also supported by the very reasonable values of the goodness-of-fit parameter for all fits. Note that even the simplest expression

$$\xi_{\rm imp} = [\hat{G}(\mathbf{0})/\hat{G}(\mathbf{1}) - 1]^{1/2} / 2\sin(\pi/L)$$

(involving *no* fit at all) can be used. Our final results for $\xi_{\rm imp}$ in Table IV are from fits using all six possible $\mathbf{k}$ values up to $\mathbf{k} = (2\pi/L)(2,1,0)$, since the error estimates trivially decrease with the number of points taken into account.

In what follows we describe the least-squares-fit techniques employed to determine the critical coupling and the exponents ν and γ from the raw data in Table IV. Although we are quite confident in the accuracy of the correlation length results, we shall first consider the susceptibility data which, *a priori*, is more reliable since no intermediate analyses are involved.

A. Susceptibility

Starting with the simplest ansatz

$$\bar{\chi}(\beta) = \bar{\chi}_0 (1 - \beta/\beta_c)^{-\gamma} , \tag{31}$$

we obtained from a nonlinear three-parameter least-squares fit to all 18 data points (using $\bar{\chi}_{\rm imp}$),

$$\beta_c = 0.692\,94 \pm 0.000\,03 , \tag{32}$$

$$\gamma = 1.391 \pm 0.003 , \tag{33}$$

$$\bar{\chi}_0 = 0.955 \pm 0.006 , \tag{34}$$

with a chi squared of $\chi^2 = 7.83$, corresponding to a goodness-of-fit parameter $Q = 0.93$, which clearly justifies *a posteriori* the ansatz (31). The very precise estimate for β_c is only little lower than our previous value (19),

$\beta_c=0.6930(1)$, derived from FSS analyses of the U_L crossing points. The exponent γ agrees very well with the field-theoretical estimates $\gamma=1.386(4)$ (resummed perturbation series[43]), $\gamma=1.390(10)$ (resummed ε expansion[44]). The amplitude $\bar{\chi}_0$ is close to the mean-field value $\bar{\chi}_0^{\mathrm{MF}}=1$ and agrees surprisingly well with old analyses of nine-term high-temperature series (HTS) expansions by Ritchie and Fisher[39] (RF), which gave $\bar{\chi}_0^{\mathrm{RF}}=0.96647(5)$ [using $\beta_c^{\mathrm{RF}}=0.6916(2)$ and $\gamma^{\mathrm{RF}}=1.38(2)$ as input]. We could not trace any more recent published number to compare with. From the HTS analyses in Ref. 40, however, it is straightforward to derive another comparative value for $\bar{\chi}_0$. Expanding the ansatz for the dominant singularity (31) into a power series in β, inserting the estimates for the critical parameters given in Table 4 of Ref. 40, $\beta_c=0.6924(2)$, $\gamma=1.387(4)$ (Padé approximants) and $\beta_c=0.6925(1)$, $\gamma=1.395(5)$ (ratio method), and comparing with the coefficients of the HTS expansion,[40,46] we obtain a sequence of amplitude values that stabilize with increasing order of the expansion at $\bar{\chi}_0^{\mathrm{HTS}}\approx 0.9508$ and $\bar{\chi}_0^{\mathrm{HTS}}\approx 0.9326$, respectively. Moreover, using our values (32) and (33) for β_c and γ, we obtain by the same procedure a very smooth sequence for $\bar{\chi}_0$, yielding asymptotically $\bar{\chi}_0=0.9501$. The smoothness indicates that the simplest ansatz (31), together with our estimates (32)–(34), represents an excellent extrapolation of the HTS expansion, whose quality is comparable (if not better) with the results given in Ref. 40.

As a further self-consistency check of the range of validity of the ansatz (31), we tested for the asymptotic scaling region by successively discarding more and more data points with small correlation length. As is demonstrated in Fig. 11 for β_c, only a weak downward trend is observable, which, compared to the error bars, is hardly significant. We can thus conclude that the ansatz (31) passes all usual self-consistency checks and that the estimates (32)–(34) should thus be reliable.

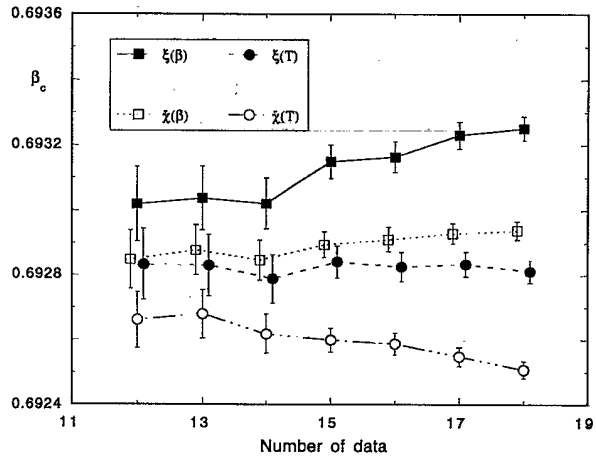

FIG. 11. Critical coupling β_c as estimated from nonlinear three-parameter fits to ξ and $\bar{\chi}$ assuming the leading power-law singularity only, written as function of β or T. The x axis shows how many data points are taken into account in these fits (i.e., from right to left more and more points with small correlation length are discarded). In order to disentangle the error bars, two curves are slightly displaced in x.

It is of course surprising that the simplest ansatz (31) works even for data points with correlation lengths as small as $\xi\approx 3$. Theoretically, we would have expected to see *confluent* correction terms of the type $\bar{\chi}_{\mathrm{conf}}(1-\beta/\beta_c)^{-\gamma+\Delta_1}$, where $\Delta_1=\omega\nu\approx 0.55$ (Refs. 43, 44, and 47) is the confluent correction exponent[48] and *analytic* correction terms of the Darboux type, $\bar{\chi}_{\mathrm{anal}}(1-\beta/\beta_c)^{-\gamma+1}$, leading to the more general ansatz

$$\bar{\chi}(\beta)=\bar{\chi}_0(1-\beta/\beta_c)^{-\gamma}+\bar{\chi}_{\mathrm{conf}}(1-\beta/\beta_c)^{-\gamma+\Delta_1}+\bar{\chi}_{\mathrm{anal}}(1-\beta/\beta_c)^{-\gamma+1}\ . \tag{35}$$

Including both correction terms as free parameters into the fit routine is a hopeless enterprise. Instead, we first tried fits with β_c held *fixed* at values around 0.692 90 in steps of 0.000 01, and γ, $\bar{\chi}_0$, $\bar{\chi}_{\mathrm{conf}}$, and $\bar{\chi}_{\mathrm{anal}}$ as free parameters. The quality of the fits remained high for a large range of β values. The best fit with $Q=0.97$ was obtained for $\beta_c=0.692\,81$ and gave $\gamma=1.365(25)$, $\bar{\chi}_0=1.06(17)$, $\bar{\chi}_{\mathrm{conf}}=-0.11(79)$, and $\bar{\chi}_{\mathrm{anal}}=-0.25(1.18)$. We see that the correction terms come out to be consistent with zero, but that the error bars are fairly large as a result of the increased number of free parameters, so that no definite conclusion can be drawn from these fits.

We therefore decided to perform two further types of fits. First, we added to the leading term in (35) only the analytic correction term (i.e., we enforced the amplitude of the confluent correction term to be zero), and second, we tried to use only the confluent correction term with fixed $\Delta_1=0.55$ (i.e., we put the amplitude of the analytic correction equal to zero). Fitting thus all 18 data points to the ansatz (35) with either $\bar{\chi}_{\mathrm{conf}}$ or $\bar{\chi}_{\mathrm{anal}}$ held fixed at zero, we get for the other amplitude $\bar{\chi}_{\mathrm{anal}}=-0.40(27)$ or $\bar{\chi}_{\mathrm{conf}}=-0.35(26)$, respectively. The Q value improves only marginally, and the amplitudes are still almost consistent with zero. The other parameters change slightly, but, because of the much larger error bars than for the simple fit (31), they are still compatible.

The latter fits are nonlinear four-parameter fits which are usually quite difficult to stabilize. To cope with this problem, we followed Ref. 11 and used the following method. For any pair of values β_c,γ, we first minimized in the linear parameters $\bar{\chi}_0$ and $\bar{\chi}_{\mathrm{anal}}$ (or $\bar{\chi}_{\mathrm{conf}}$), which can be done exactly (up to round-off errors). This yields a chi-squared function

$$\chi^2(\beta_c,\gamma,\bar{\chi}_0(\beta_c,\gamma),\bar{\chi}_{\mathrm{anal}}(\beta_c,\gamma))=\chi^2(\beta_c,\gamma)\ ,$$

which depends on two nonlinear parameters only and can be minimized reliably by standard subroutines. Finally, we used the so-determined estimates of $\beta_c,\gamma,\bar{\chi}_0,\bar{\chi}_{\mathrm{anal}}$ (or $\bar{\chi}_{\mathrm{conf}}$) as initialization of the nonlinear-fit routine MRQMIN of Ref. 42, which yields then slightly improved parameter values and standard error estimates. The fits with γ, $\bar{\chi}_0$, $\bar{\chi}_{\mathrm{conf}}$, and $\bar{\chi}_{\mathrm{anal}}$ as free parameters were performed similarly.

One can also rewrite Eq. (35) as a function of T,

$$\bar{\chi}(T)=\bar{\chi}'_0(T/T_c-1)^{-\gamma}+\bar{\chi}'_{\rm conf}(T/T_c-1)^{-\gamma+\Delta_1}+\bar{\chi}'_{\rm anal}(T/T_c-1)^{-\gamma+1}\ , \tag{36}$$

with $\bar{\chi}'_0=\bar{\chi}_0$, $\bar{\chi}'_{\rm conf}=\bar{\chi}_{\rm conf}$, and $\bar{\chi}'_{\rm anal}=\bar{\chi}_{\rm anal}+\gamma\bar{\chi}_0$. This form is obtained from (35) by a simple change of variable $\beta\to 1/T$, expanding around T_c, and keeping the same correction terms. We believe that (36) with $\bar{\chi}'_{\rm conf}=\bar{\chi}'_{\rm anal}=0$ is, *a priori*, as justified as the simplest β-dependent ansatz (31). Since HTS analyses are based on expansions in β, there is definitely a bias to prefer the ansatz (31). We are not aware, however, of a mathematically sound justification for this choice. For what we think is a counterexample, see our correlation-length analysis below.

Because the simplest β-dependent ansatz (31) works so good, it is thus clear that for the temperature-dependent-fit ansatz we have to take into account the analytic correction term. As anticipated, trying to fit the simplest ansatz (36) with $\bar{\chi}'_{\rm conf}=\bar{\chi}'_{\rm anal}=0$ to all 18 data points results in a fit with a comparatively poor chi squared of $\chi^2=21.66$, corresponding to $Q=0.12$. By again successively discarding the data points with small correlation length, the quality of the fit improves rapidly, and in Fig. 11 we see a weak trend that the values of β_c from the two types of fits may approach each other asymptotically.

The fit to all 18 data points with $\bar{\chi}'_{\rm anal}$ as a free parameter agrees perfectly with the corresponding β-dependent ansatz (also with $\bar{\chi}_{\rm anal}$ as a free parameter), yielding the expected correction amplitude $\bar{\chi}'_{\rm anal}=1.03(26)$. The fit with $\bar{\chi}'_{\rm conf}$ as a free parameter is only slightly worse. The value of $\bar{\chi}'_{\rm conf}=0.90$ (instead of the expected result $\bar{\chi}'_{\rm conf}=\bar{\chi}_{\rm conf}\approx 0$) indicates, however, that in this case the confluent correction term tries to account for the suppressed analytic correction term and that it can indeed mimic the analytic behavior very well.

The main result of all our efforts is that on the basis of standard statistical tests the simple ansatz (31) *turns out* to be justified. We emphasize this point because *a priori* it is not at all clear that the confluent correction is extremely small and that also the analytic correction is negligible if the proper variable (β in the case of $\bar{\chi}$) is chosen. Although we feel that the corrections cannot completely be ignored, one would need more accurate data to account for these corrections in a reliable way.

B. Correlation length

We have repeated the same type of analysis for the correlation-length data. Starting again with the simplest possible ansatz, taking into account only the leading singularity, we find this time that the temperature-dependent ansatz

$$\xi(T)=\xi'_0(T/T_c-1)^{-\nu} \tag{37}$$

is well behaved. It should be emphasized that, as far as the role of β and T is concerned, this is just opposite to the situation for the susceptibility. The fit to all 18 data points in Table IV yields

$$\beta_c=0.692\,81\pm 0.000\,04\ , \tag{38}$$

$$\nu=0.698\pm 0.002\ , \tag{39}$$

$$\xi'_0=0.484\pm 0.002\ , \tag{40}$$

with a chi squared of $\chi^2=8.14$, corresponding to a goodness-of-fit parameter $Q=0.92$, which may again be taken as *a posteriori* justification of the simple ansatz (37). The estimate for β_c is somewhat smaller than the previous estimates and also the exponent ν is only barely compatible with our FSS value $\nu=0.704(6)$ and with the field-theoretical estimates $\nu=0.705(3)$ (resummed perturbation series[43]), $\nu=0.710(7)$ (resummed ε expansion[44]), but it still lies within the 2σ error interval of these estimates. If we extract ξ from fits through the four lowest $\mathbf{k}$ values only, we obtain the same central values as in (38)–(40) with about 1.5 times bigger error bars and a Q value of 0.99. In Fig. 11 we see that fits with the ansatz (37) are very stable against discarding more and more data points with small correlation length.

Correspondingly, if we include into the T-dependent ansatz one correction term at a time, as described in the susceptibility analysis, we obtain amplitudes that are fully consistent with zero, $\xi'_{\rm conf}=-0.048(65)$ and $\xi'_{\rm anal}=-0.065(76)$. For the corresponding β-dependent fit, we thus expect $\xi_{\rm conf}\approx 0$ and $\xi_{\rm anal}=\xi'_{\rm anal}-\nu\xi'_0=-0.267$. The latter value is extremely well reproduced by the β-dependent fit with analytic correction term [$\xi_{\rm anal}=-0.272(76)$]. Similar to the susceptibility, the confluent amplitude, however, comes out much too large in an attempt to mimic the analytic correction term. We can thus conclude that also for the correlation length confluent corrections are negligible. Analytic correction terms are important in the β-dependent ansatz but negligible in the T-dependent ansatz, just opposite to the situation for the susceptibility.

It is noteworthy that, using correction terms, the value of ν slightly increases, just opposite to the case of the susceptibility data, where the value of γ decreases when corrections are included. It is impossible to find an objective criterion for the systematic errors but with what we experienced, we feel that they are at least of the order of the statistical errors, in particular for the susceptibility, where the correction terms seem to be somewhat more important than for the correlation length.

Combining the estimates for β_c from the susceptibility and correlation length data in the high-temperature phase, we obtain a final estimate of

$$\beta_c=0.692\,88\pm 0.000\,04\ , \tag{41}$$

which is slightly smaller than our crossing value of 0.6930(1), but in agreement with the MC estimate by Peczak, Ferrenberg, and Landau.[23]

C. Exponent η

Finally, we have combined the scaling behavior of ξ and $\bar{\chi}$ to get a direct estimate of the exponent $\eta=2-\gamma/\nu$ from the relation $\bar{\chi}\propto\xi^{\gamma/\nu}$ or

$$\ln(\bar{\chi}/\xi^2)=c-\eta\ln\xi\ , \tag{42}$$

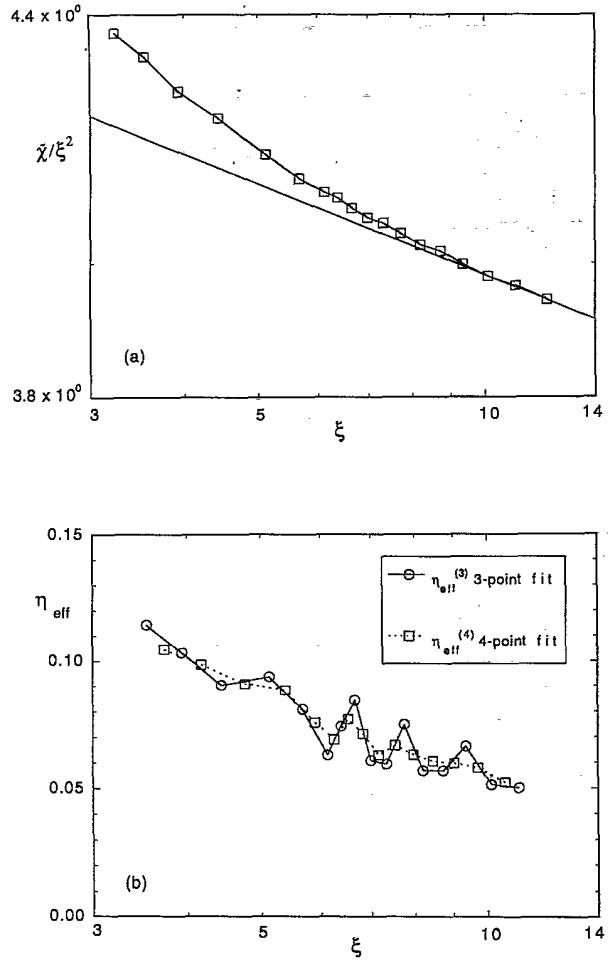

FIG. 12. (a) Log-log plot of $\bar{\chi}/\xi^2$ vs ξ. The slope of the linear envelope for large ξ gives $\eta \approx 0.05$. (b) The effective critical exponent η_{eff} vs ξ on a logarithmic scale, using two different discretization schemes. The asymptotic value of η_{eff} as $\xi \to \infty$ is an estimate for the critical exponent $\eta = 2 - \gamma/\nu$.

where c is a constant. By plotting $\bar{\chi}/\xi^2$ vs ξ on a log-log scale as in Fig. 12(a), we thus expect asymptotically for large ξ a straight line with slope $-\eta$. We see that up to $\xi \approx 12$ our data still give a curved line, indicating that corrections to asymptotic scaling cannot yet be neglected. Taking a linear envelope to the last few points as rough estimate, we obtain $\eta \approx 0.05$. Alternatively, we can define an effective exponent

$$\eta_{\text{eff}}^{(2)} = -\ln(\bar{\chi}_{i+1}\xi_i^2/\bar{\chi}_i\xi_{i+1}^2)/\ln(\xi_{i+1}/\xi_i)$$

as the local slope between two points in Fig. 12(a). Since this gives quite noisy results, we have actually computed the local slopes from linear fits through three and four points, denoted by $\eta_{\text{eff}}^{(3)}$ and $\eta_{\text{eff}}^{(4)}$, respectively. These effective exponents are plotted versus ξ on a logarithmic scale in Fig. 12(b). Again, we see that up to correlation lengths of the order of $\xi \approx 12$ the effective exponents have clearly not yet reached the asymptotic value ($=\eta$). However, assuming a monotonic behavior as $\xi \to \infty$, we get at least an upper bound $\eta < 0.05$. Recall the field-theory values, which are $\eta = 0.033(4)$ (resummed perturbation series[43]), $\eta = 0.040(3)$ (resummed ε expansion[44,49]). Estimates for the other critical exponents can be derived using (hyper) scaling laws. We obtain $\beta = \frac{3}{2}\nu - \frac{1}{2}\gamma = 0.352(4)$ and $\alpha = 2 - 3\nu = -0.094(6)$ (compare also Table V).

V. CONCLUDING REMARKS

In conclusion, we have shown that the *single*-cluster update eliminates critical slowing down for the three-dimensional Heisenberg model almost completely. As for the 3D Ising and XY models, we expect that it is more efficient than the *multiple*-cluster algorithm, but this has not yet been explicitly verified because of the lack of data for the multiple-cluster algorithm. Combined with histogram reweighting and optimization techniques, finite-size scaling analyses allow a precise Monte Carlo determination of the critical exponents of the 3D Heisenberg model, whose accuracy is comparable with the best estimates coming from field-theoretical methods. Direct analyses of thermodynamic measurements based on improved estimators in the high-temperature phase yield compatible

TABLE V. Various sources for estimates of the critical parameters for the classical 3D Heisenberg model. For the MC simulations scaling relations were used to obtain estimates for α (all) and β (only HT), and the FSS values of the exponents γ and β were calculated from the measured ratios, using the estimate for ν. The field-theory estimates of ratios with ν are calculated from the values and errors of the critical exponents.

	Field theory		MC simulations		
Critical parameter	g expansion Ref. 43	ε expansion Refs. 38 and 44	Metropolis MC Ref. 23	This study FSS	HT
β_c			0.6929(1)	0.6930(1)	0.69288(4)
U^*		0.59684	0.622(1)	0.6217(8)	
ν	0.705(3)	0.710(7)	0.706(9)	0.704(6)	0.698(2)
α	−0.115(9)	−0.130(21)	−0.118(27)	−0.112(18)	−0.094(6)
α/ν	−0.163(12)	−0.183(28)	−0.167(36)	−0.159(24)	−0.135(9)
β	0.3645(25)	0.368(4)	0.364(7)	0.362(4)	0.352(4)
β/ν	0.517(6)	0.518(11)	0.516(3)	0.514(1)	0.504(5)
γ	1.386(4)	1.390(10)	1.390(23)	1.389(14)	1.391(3)
η	0.033(4)	0.040(3)	0.031(7)	0.027(2)	<0.05

results. For the reader's convenience we have compiled some relevant sources on the critical parameters of the classical 3D Heisenberg model in Table V. Overall, our results are in good agreement with the Monte Carlo values reported recently by Peczak, Ferrenberg, and Landau.[23] In particular we confirm that the value for β_c on a simple cubic lattice is significantly higher than previous estimates coming from analyses of high-temperature series expansions. We would like to remark, however, that a very recent analysis[52] of extended series expansions[53] (up to 14th order), using more refined Padé-approximant techniques, is consistent with the MC estimates.

ACKNOWLEDGMENTS

The numerical simulations were performed on the CRAY X-MP and Y-MP computers of the Konrad-Zuse Zentrum für Informationstechnik Berlin (ZIB), the CRAY X-MP computer at the Rechenzentrum der Universität Kiel, and in the late stage of the project, also on the CRAY Y-MP computer of the Höchstleistungsrechenzentrum (HLRZ), Forschungszentrum Jülich. We thank all institutions for their generous support. This work was supported in part by Deutsche Forschungsgemeinschaft under Grant No. Kl256.

[1]K. Binder, *Monte Carlo Methods in Statistical Physics,* edited by K. Binder (Springer, New York, 1979), p. 1. See also the articles in *Finite-Size Scaling and Numerical Simulations of Statistical Systems,* edited by V. Privman (World Scientific, Singapore, 1990).

[2]For reviews, see, e.g., R. H. Swendsen, J.-S. Wang, and A. M. Ferrenberg, in *The Monte Carlo Method in Condensed Matter Physics,* edited by K. Binder (Springer, Berlin, 1991); C. F. Baillie, Int. J. Mod. Phys. C **1**, 91 (1990); A. D. Sokal, *Monte Carlo Methods in Statistical Mechanics: Foundations and New Algorithms,* Cours de Troisième Cycle de la Physique en Suisse Romande, Lausanne, 1989.

[3]M. E. Barber, in *Phase Transitions and Critical Phenomena,* edited by C. Domb and J. L. Lebowitz (Academic, New York, 1983), Vol. 8.

[4]R. H. Swendsen and J.-S. Wang, Phys. Rev. Lett. **58**, 86 (1987); J.-S. Wang and R. H. Swendsen, Physica A **167**, 565 (1990).

[5]U. Wolff, Phys. Rev. Lett. **62**, 361 (1989).

[6]U. Wolff, Phys. Lett. B **228**, 379 (1989).

[7]P. Tamayo, R. C. Brower, and W. Klein, J. Stat. Phys. **58**, 1083 (1990).

[8]D. W. Heermann and A. N. Burkitt, Physica A **162**, 210 (1990).

[9]U. Wolff, Nucl. Phys. **B322**, 759 (1989).

[10]R. G. Edwards and A. D. Sokal, Phys. Rev. D **40**, 1374 (1989).

[11]W. Janke and K. Nather, Phys. Lett. A **157**, 11 (1991).

[12]W. Janke and K. Nather, in *Computer Simulations Studies in Condensed Matter Physics IV,* edited by D. P. Landau *et al.* (Springer, Berlin, in press); Nucl. Phys. **B30** (Proc. Suppl.), 834 (1993).

[13]U. Wolff, Phys. Lett. B **222**, 473 (1989).

[14]U. Wolff, Nucl. Phys. **B334**, 581 (1990).

[15]U. Wolff, Phys. Lett. B **248**, 335 (1990).

[16]J.-S. Wang, Physica A **164**, 240 (1990).

[17]M. Hasenbusch and S. Meyer, Phys. Lett. B **241**, 238 (1990).

[18]W. Janke, Phys. Lett. A **148**, 306 (1990).

[19]C. Holm and W. Janke, Phys. Lett. A **173**, 8 (1993); C. Holm and W. Janke, Nucl. Phys. **B30** (Proc. Suppl.), 846 (1993).

[20]Y. Miyatake, M. Yamamoto, J. J. Kim, M. Toyonaga, and O. Nagai, J. Phys. C **19**, 2539 (1986).

[21]M.-h. Lau and C. Dasgupta, J. Phys. A **21**, L51 (1988); Phys. Rev. B **39**, 7212 (1989).

[22]For further references to early work in the 1960s and 1970s, see Ref. 23.

[23]P. Peczak, A. M. Ferrenberg, and D. P. Landau, Phys. Rev. B **43**, 6087 (1991).

[24]P. Peczak and D. P. Landau, J. Appl. Phys. **67**, 5427 (1990).

[25]For an extensive list of references, see the erratum in Ref. 26.

[26]A. M. Ferrenberg and R.H. Swendsen, Phys. Rev. Lett. **61**, 2635 (1988); **63**, 1658 (E) (1989).

[27]A. M. Ferrenberg and R. H. Swendsen, Phys. Rev. Lett. **63**, 1195 (1989).

[28]M. Falcioni, E. Marinari, M. L. Paciello, G. Parisi, and B. Taglienti, Phys. Lett. **108B**, 331 (1982); E. Marinari, Nucl. Phys. **B235**, 123 (1984); G. Bhanot, S. Black, P. Carter, and R. Salvador, Phys. Lett. B **183**, 331 (1987); P. B. Bowen, J. L. Burke, P. G. Corsten, K. J. Crowell, K. L. Farrell, J. C. MacDonald, R. P. MacDonald, A. B. MacIsaac, P. H. Poole, and N. Jan, Phys. Rev. B **40**, 7439 (1989); E. P. Münger and M. A. Novotny, *ibid.* **43**, 5773 (1991).

[29]N. Madras and A. D. Sokal, J. Stat. Phys. **50**, 109 (1988).

[30]M. B. Priestley, *Spectral Analysis and Time Series* (Academic, London, 1981); Chaps. 5–7.

[31]T. W. Anderson, *The Statistical Analysis of Time Series* (Wiley, New York, 1971).

[32]This can be read off from Fig. 2 in Ref. 24.

[33]As well as from storing the full time series of E and M, which conceptually would be even simpler.

[34]Because of technical reasons, we had four simulations for the lattices $L=24$ and 48; compare also Table I.

[35]R. G. Miller, Biometrika **61**, 1 (1974); B. Efron, *The Jackknife, the Bootstrap and other Resampling Plans* (SIAM, Philadelphia, PA, 1982).

[36]A similar procedure was used in N. A. Alves, B. A. Berg, and S. Sanielevici, Nucl. Phys. **B376**, 218 (1992).

[37]K. Binder, Z. Phys. B **43**, 119 (1981).

[38]E. Brézin and J. Zinn-Justin, Nucl. Phys. **B257** [FS14], 867 (1985).

[39]D. S. Ritchie and M. E. Fisher, Phys. Rev. B **5**, 2668 (1972).

[40]S. McKenzie, C. Domb, and D. L. Hunter, J. Phys. A **15**, 3899 (1982).

[41]A. M. Ferrenberg and D. P. Landau, Phys. Rev. B **44**, 5081 (1991).

[42]W. H. Press, B. P. Flannery, S. A. Teukolsky, and W. T. Vetterling, *Numerical Recipes—The Art of Scientific Computing* (Cambridge University Press, Cambridge, England, 1986).

[43]J. C. Le Guillou and J. Zinn-Justin, Phys. Rev. B **21**, 3976 (1980).

[44]J. C. Le Guillou and J. Zinn-Justin, J. Phys. (Paris) Lett. **46**, L137 (1985).

[45]Th. T. A. Paauw, A. Compagner, and D. Bedaux, Physica A **79**, 1 (1975).

[46]G. S. Rushbrooke, G. A. Baker, Jr., and P. J. Woods, in *Phase Transitions and Critical Phenomena,* Vol. 3, edited by C. Domb and M. S. Green (Academic, New York, 1974), p. 245.

[47]The precise values are $\omega=0.78(2)$, $\Delta_1=0.55(3)$ (Ref. 43); $\omega=0.79(4)$, $\Delta_1=0.56(4)$ (Ref. 44).

[48]F. J. Wegner, Phys. Rev. B **5**, 4529 (1972).

[49]In a recent recalculation (Ref. 50) of all Feynman graphs contributing to the highest order of the ε expansion [$\mathcal{O}(\varepsilon^5)$], several errors were corrected. A subsequent reanalysis (Ref. 51) of the resummed series gave a slightly smaller value for η. Compared with the error bar, however, this change is negligible.

[50]H. Kleinert, J. Neu, V. Schulte-Frohlinde, K. G. Chetyrkin, and S. A. Larin, Phys. Lett. B **272**, 39 (1991).

[51]W. Janke and H. Kleinert (unpublished).

[52]J. Adler, C. Holm, and W. Janke, Physica A (to be published).

[53]M. Lüscher and P. Weisz, Nucl. Phys. **B300**, 325 (1988).